A novel heterogeneous catalyst for synthesis of dimethyl carbonate by transesterification

Tong Wei, Mouhua Wang, Wei Wei, Yuhan Sun, Bing Zhong*

State Key Laboratory of Coal Conversion,
Institute of Coal Chemistry,
Chinese Academy of Sciences,
Taiyuan, 030001, P.R.China

Introduction

Dimethyl carbonate (DMC) is an important precursor of polycarbonate resins as well as a useful carbonylation and methylation agent [1]. Because of the negligible toxicity of DMC, it is promising as a substitute for phosgene, dimethyl sulfate, or methyl iodide. DMC can be prepared by the oxidative carbonylation of methanol, carbonylation of methyl nitrite or transesterification of cyclic carbonate with methanol [2,3]. Because of the moderate reaction conditions and the use of CO_2 as raw material, transesterification method, as shown follow, has gained increasing attention in recent years [4]. In our previous work, CaO prepared from the dissociation of $CaCO_3$ at elevated temperature was found very effective for synthesis of DMC from methanol and propylene carbonate, even at room temperature [5]. However, ultra fine CaO prepared from $CaCO_3$ are difficult to be separated from the products and reused. Therefore, CaO-carbon composites were prepared in present paper; the structure, basicity and the catalytic performance of such catalyst were also investigated.

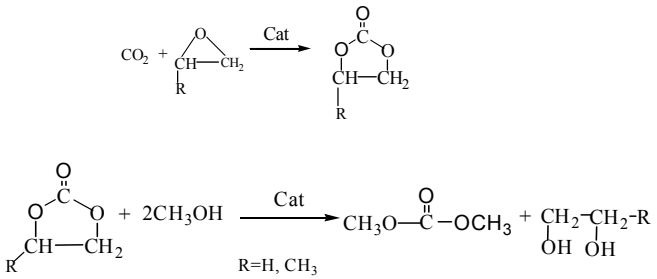

Experimental

CaO was prepared by heating $CaCO_3$ at 1173K for 1 h in N_2 atmosphere. CaO-C composite was prepared from phenolic and $CaCO_3$ (weight ratio=5:1:5), which were grounded and mixed homogeneously. The mixture then was pumped at 20 MPa and solidified at 473K for 10 h in N_2 atmosphere. After being broken into small particles ranging from 60 to 80 mesh, the solidified mixture was activated at 1173K for 1 h in N_2 atmosphere to prepare final catalyst (CaO-C composite, CaO: 50 wt%). The reaction was carried out in a 250 mL flask equipped with reflux condenser, water bath and strong magnetic stirring. The mole ratio of MeOH to PC for all evaluation reaction was 4:1, and the catalyst used were 0.90 wt% (CaO) or 1.80 wt% (CaO-C). The product was analyzed on a gas chromatograph with a TCD after centrifugal separation from the catalyst.

Result and discussion

The XRD shows that the structure of CaO in CaO-C composite hardly changes (both are cubic CaO). As a result, the basic property of CaO-C almost remains as that of pure CaO, which is illustrated by CO_2-TPD of CaO and CaO-C (see **Figure 1**). This indicates that no chemical interaction takes place between carbon and CaO, and carbon mainly acts as the inert supporter. The pore distributions of CaO-C and carbon are illustrated in **Figure 2**. It can be seen that although there are two kinds of pores, micropores and mesopors in CaO-C samples, only mesopores are effective for the catalysis of CaO loaded on carbon.

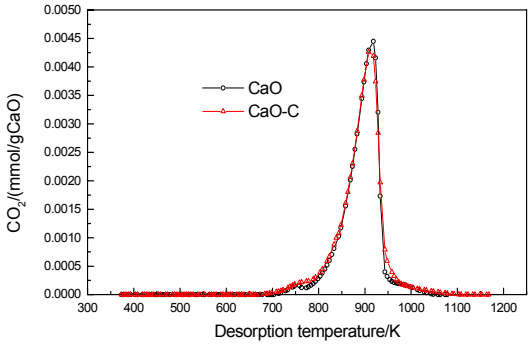

Figure1 CO_2 TPD of CaO and CaO-C

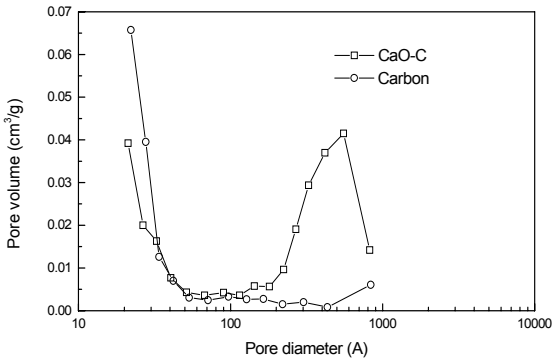

Figure 2 Pore distribution of CaO -C and carbon

The catalytic performance of CaO-C is illustrated in **Figur 3**, and that of CaO is also given for comparison. For CaO-C as catalyst, with the rise of temperature, reaction rate increase greatly, the reaction reach equilibrium in 60 min at 323K. Whereas, the reaction rate over CaO-C catalyst is still slower than that over pure CaO. Because the crystal structure, base strength and basicity of CaO-C are similar to that of pure CaO, the catalytic performance difference between CaO and CaO-C may come from the mass transfer of them. CaO used in this paper are ultra fine particles with diameter about 10-20nm, and the reaction mainly proceeds on the surface of the powders under strong mixing. Thus the reaction rate is intrinsic. Whereas the CaO-C catalyst used is particles of 60~80 mesh, the reaction, therefore, proceeds on outer surface and especially inner surface. Furthermore, this reaction proceeds in liquid phase and the viscosity of reactants and products especially that of propylene glycol are very high under low temperature, which make reactant and product molecules, particularly propylene glycol move very slowly in the pores of CaO-C catalyst. To illustrate the reusability of the catalyst, CaO-C was reused two times (see **Figure 4**), after each reaction the catalyst was separated by filtration and reused. It can be seen that the catalytic activity hardly changes when CaO-C catalyst is used for three times.

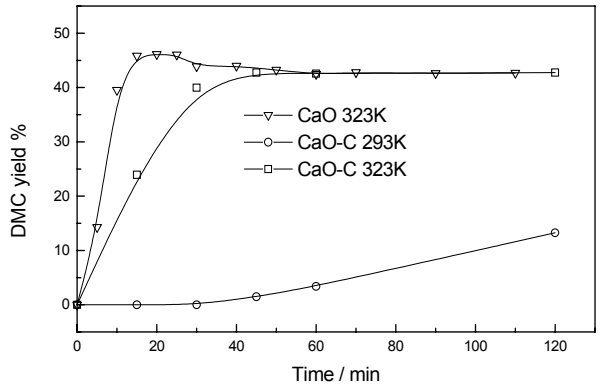

Figure 3 Catalytic performance of pure CaO and 50% wt CaO-C with the same CaO content.

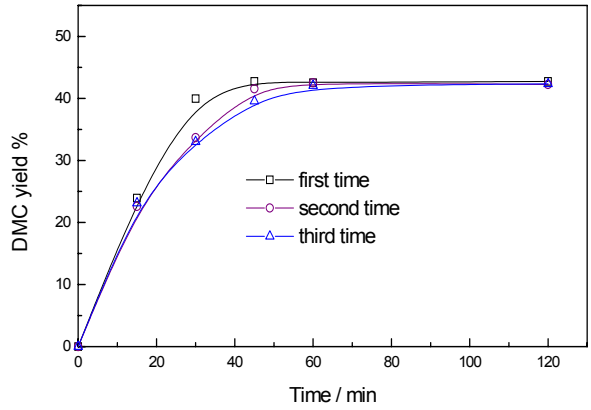

Figure 4 Reusability of CaO-C for synthesis of DMC. temperature: 323K

Conclusion

In conclusion, CaO-carbon composite serves as an efficient and convenient heterogeneous catalyst for synthesis of dimethyl carbonate from methanol and propylene carbonate. Compared with pure CaO, the CaO-C shows the same basic property and then high performance. Furthermore, the catalyst is easily recovered and reused without a significant loss of its efficiency.

References

(1) Sato Y.; Yamamoto T.; Souma Y. *Catal. Letters,* **2000**, 65**,** 123.
(2) Pacheco M. A.; Marshall C. L. *Energy & Fuels,* **1991**, 11**,** 2.
(3) Fujita S.; Bhanage B. M.; Ikushima Y. and Arai M. *Green Chemistry,* **2001**, 3**,** 87.
(4) Ikedal Y.; Sakaihori T.; Tomishige K.; Fujimoto K. *Catal. Letters*, **2000**, 66**,** 59.
(5) Wei T.; Wang M.; Wei W.; Sun Y. and Zhong B. *Preprints of Fuel Chemistry,* **2002**, 312.

DEGRADATION OF AQUEOUS ALKANOLAMINE SOLUTIONS CONTAINING CO_2 AND H_2S

Kwang-Joong Oh[1], Sang-Sup Lee[1], Byung-Hyun Shon[2], Sang-Wook Park[3], and Dae-Won Park[3]

(1) Department of Environmental Engineering, Pusan National University, Pusan, 609-735, Korea (2) Department of Environmental Engineering, Hanseo University, Choongnam, 356-820, Korea (3) Department of Chemical Engineering, Pusan National University, Pusan, 609-735, Korea

Introduction

The removal of CO_2 and H_2S from natural, refinery, and synthesis gas stream plays an important role in gas processing. Aqueous alkanolamine solutions are frequently used for the removal of CO_2 and H_2S, and the alkanolamines include MEA (monoethanol-amine), DIPA (diisopropanolamine), DEA (diethanolamine), MDEA (*N*-methyldiethanolamine). Recently, the sterically hindered amine such as AMP (2-amino-2-methyl-1-propanol) has been suggested as an attractive solvent for the removal of acid gases, and the advantage of AMP includes high equilibrium loading capacity (1.0mol of CO_2 per mole of amine). In addition, aqueous MDEA solution is frequently used as a solvent for selectively absorbing H_2S because of its instantaneous reaction with H_2S.

However, in removing acid gas by alkanolamines and regenerating them, undesirable compounds can be produced by the irreversible transformation of alkanolamines, which is called degradation. Degradation causes a loss of alkanolamine, and it may also contribute to operational problems such as foaming, corrosion and fouling. To understand the mechanism of degradation and to find the method to suppress it is required.

In this study, AMP 30wt%+MDEA 3wt%, which had high absorption capacity of CO_2 and H_2S in former study, AMP 30wt%, MDEA 30wt%, and DEA 30wt% were degraded in 120, 160, and 200℃ for 30days. And then, the degradation rates and degradation products of alkanolamines were measured.

Experimental

Materials and Apparatus. AMP (99%) was purchased from Acros, MDEA (99%) was from Tokyo chemical, and DEA (99%) was from Katayama chemical. The carbon dioxide (99.9%), the nitrogen (99.99%), and the hydrogen sulfide (99.9%) were obtained from Daeyounggas Co.(Korea).

The reactor was made of stainless steel with about 10cm^3 volume (13cm height, 1cm diameter). We poured silicon oil into oil bath and then heating oil bath with temperature controller to maintain the reaction temperature, and confirmed the temperature by thermometer.

Procedure. We prepared all the solutions with distilled water and then made 6wt% CO_2 and H_2S absorbed into the solutions respectively by using absorption instrument. After we poured 5ml of the solutions into reactor, we heated the reactor to 120, 160, and 200℃. The degraded solutions were acquired for scheduled days, and analyzed by GC (DS6200). The GC (DS6200) was composed of FID (Flame Ionization Detector) and packed column (Tenax TA 60-80mesh, 1/8in. O.D., and 9ft. long). The operating conditions of GC were as follows; Helium gas was carried at 20ml/min flow rate, and oven temperature was increased from 150 to 300℃ by 6℃/min rate, and maintained at 150℃ for 0.5 minutes and at 300℃ for 3 minutes. The temperature of injector and detector was 300℃ and 1μl of degraded solution was instilled by a syringe.

Results and Discussion

When AMP 30wt%+MDEA 3wt% solution containing 6wt% CO_2 was degraded at 120, 160, and 200℃, AMP concentration of the solution decreased with time for the beginning part of it at constant rate as shown in **Figure 1**. Therefore, initial degradation can be assumed as first order reaction as Polderman and Steele presented in their study. After degradation in three kinds of temperature for 10 days, the concentrations of AMP decreased to about 83% of basal AMP concentration at 120℃, 67% at 160℃, and 31% at 200℃.

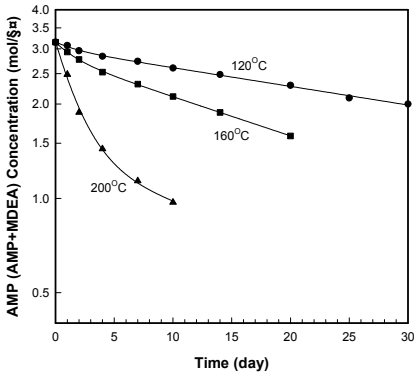

Figure 1. AMP concentration as a function of time and temperature. (AMP 30wt%+MDEA 3wt%+H_2O 61wt%+CO_2 6wt%).

6wt% CO_2 was absorbed into the aqueous alkanolamine solutions such as AMP, MDEA, and DEA, and then the solutions were degraded at 120, 160, and 200℃ respectively. Initial degradation rate constants could be measured with degradation temperature, and **Figure 2** shows this result by Arrhenius plots. Initial degradation rate constants of AMP 30wt% solutions containing 6wt% CO_2 were 0.0212, 0.0801 and 0.2481day^{-1} and those of MDEA 30wt% solutions were 0.0331, 0.1254 and 0.3151day^{-1}.

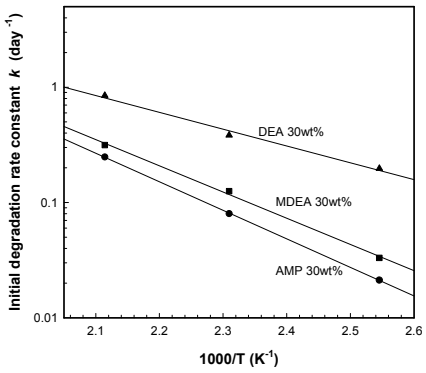

Figure 2. Arrhenius plots for k at various alkanolamines degraded with CO_2.

The constants were much lower values than those of DEA 30wt% solutions (0.1972, 0.3841 and 0.8470day^{-1}at 120, 160, and 200℃ respectively). It is considered that AMP 30wt% and MDEA 30wt%

containing 6wt% CO_2 are degraded much more slowly than DEA 30wt% are at the temperature from 120 to 200 ℃.

The addition of MDEA 3wt% into AMP 30wt% significantly increased the absorption capacity of CO_2 and H_2S in former study. Therefore, in this study, AMP 30wt%+MDEA 3wt% solutions containing 6wt% CO_2 and H_2S were degraded in 120, 200℃ and analyzed by GC, and the chromatograms are also shown in **Figure 3** and **Figure 4** respectively. **Figure 3** shows the chromatograms of the solution containing CO_2 after degradation at 120℃ for 7days and 30days. **Figure 3 (A)** shows the result of the degradation for 7days. Peak 5 is considered as AMP, peak 6 as the salt of AMP, peak 10 as MDEA, and peak 1, 13, and 14 as compounds produced by degradation. Sixteen degradation compounds were produced, and the peak areas of AMP and MDEA were decreased due to the degradation for 30days as shown in **Figure 3 (B)**.

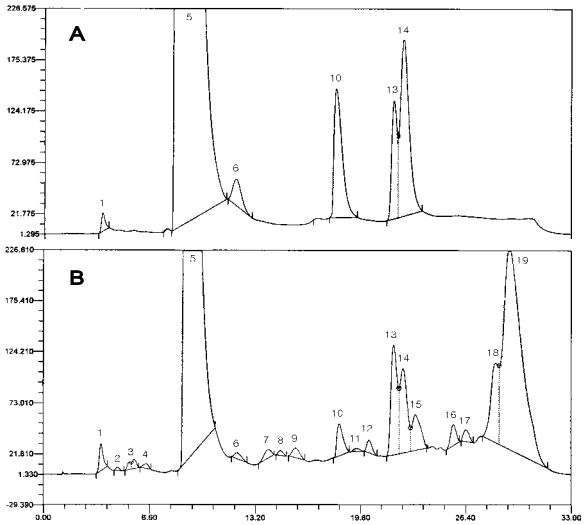

Figure 3. Chromatograms of partially degraded aqueous AMP+MDEA solutions. (AMP 30wt%+MDEA 3wt%+H_2O 61wt%+CO_2 6wt%, (A) Temp. =120℃, t=7days; (B) Temp. =120℃, t=30days).

Figure 4 (A) is the chromatogram of AMP 30wt%+MDEA 3wt% containing H_2S after degradation at 120℃ for 30days. The solution containing H_2S produced an only degradation compound while the solution containing CO_2 produced sixteen degradation compounds after the degradation at 120℃ for 30days. It is considered because the amount of H_2S absorbed into alkanolamine is less than that of CO_2 due to higher solubility of H_2S into water than that of CO_2. In addition, twelve degradation compounds were produced for 1-day degradation at 200℃ as shown in **Figure 4 (B)**.

Figure 5 shows the peak area of main degradation products transformed from AMP 30wt%+MDEA 3wt% containing 6wt% CO_2 at 120℃ for 30days. The area of peak 13 was increased for about 14days, and then it was almost constant. The area of peak 14 was the largest on degradation for about 15days. In addition, that of peak 19 was significantly increased for degradation from 25days to 30days. Therefore, it is considered that the degradation product of peak 14 may be converted to that of peak 19.

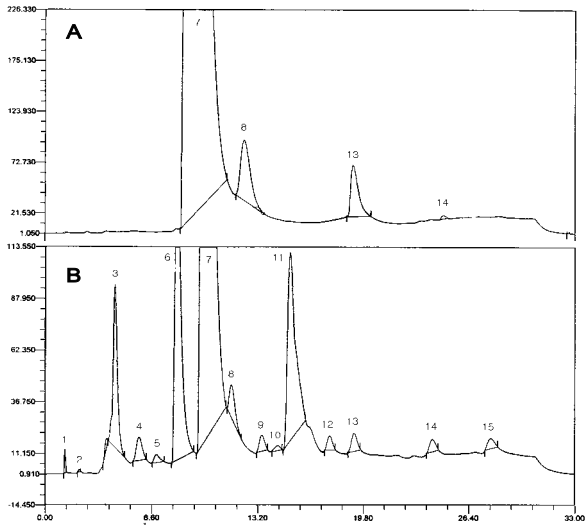

Figure 4. Chromatograms of partially degraded aqueous AMP+MDEA solutions. (AMP 30wt%+MDEA 3wt%+H_2O 61wt%+H_2S 6wt%, (A) Temp. =120℃, t=30days; (B) Temp. =200℃, t=1-day).

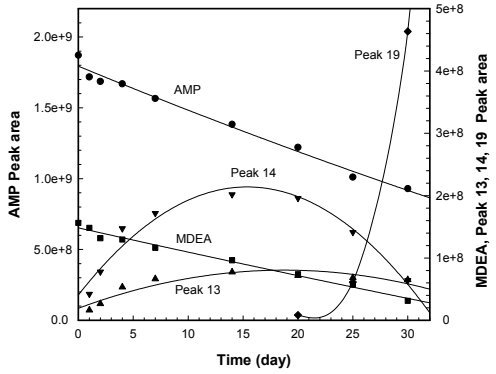

Figure 5. Rates and products of AMP+MDEA degradation. (AMP 30wt%+MDEA 3wt%+H_2O 61wt%+CO_2 6wt%, Temp. =120℃).

Acknowledgment

This work was supported by The Korean Science and Engineering Foundation under contract R01-2000-00326

References

1. Pani, F., Gaunand, A., Richon, D., Cadours, R., Bouallou, C., *J. Chem. Eng. Data*, **42**, 865～870(1997).
2. Kennard, M. L., Meisen, A., *Ind. Eng. Chem. Fundam.*, **24**, 129～140(1985).
3. Dawodu, O. F., Meisen, A., *Ind. Eng. Chem. Res.* **33**, 480～487(1994).
4. Polderman, L. D., Steele, A. B., *Oil and Gas Journal*, **54**(65), 206～214(1956).
5. Oh, K. J., Choi, W. J., Lee, J. J., Cho, S. W., Shon, B. H., *J. of KSEE*, **23**(8), 1337～1347(2001).

ENERGY FROM MACRO-ALGAE

Michele Aresta, Angela Dibenedetto and Immacolata Tommasi*

Department of Chemistry and METEA Research Center, University of Bari, Campus Universirtario, 70126, Bari – Italy.
E-mail: aresta@metea.uniba.it

Introduction

80% of the energy used today at the world level is derived from carbon based fuels, that increases the concentration of carbon dioxide in the atmosphere, rising serious concerns about the effects on global warming and climate change. To limit the emissions, alternative sources of energy have to be considered. Biomass represents an environmentally and economically feasible alternative to fossil fuels.

As a matter of fact, the forecast is that biomass may contribute to the energy balance with a share of more than 10% by 2030, with a fivefold increase with respect to the actual 2%, essentially represented by terrestrial or residual biomass utilization.

Aquatic biomass may represent a convenient solution, because it has a higher growth-rate than terrestrial plants. Micro-algae have been extensively studied so far, as they can grow both in fresh- and salty-waters [1, 2]. More recently, marine macro-algae have been considered with increasing attention [3, 4].
In this paper, the potential of macro-algae for the production of energy will be estimated.

Macro-algae for energy production

The use of macro-algae for energy production received less attention so far, despite the fact that macro-algae are cultivated since long for several purposes (food production, chemicals extraction) in China, Korea, Philippines, and Japan. The productivity is in the range 1-15 kg m^{-2} y^{-1} dry weight (10-150 t_{dw} ha^{-1} y^{-1}) for a 7-8 month culture. Either brown algae (Laminaria, Sargassum) or red algae have been used so far for such purposes.

Interestingly, macro-algae are effective in nutrients (N, P) uptake from sewage and industrial waste water, for example for the treatment of fishery effluents or agriculture drain off [5, 6]. The use of macro-algae for cleaning up effluents from fisheries is quite important as macro-algae can reduce the concentration of nitrogen derivatives like urea, amines, ammonia, nitrite or nitrate to a level that is not toxic for fishes, allowing the recycling of water. This will reduce the economic cost of growing fish as will improve the quality of the effluent water, avoiding penalties if it is discharged into the sea and making it of such quality to be recycled into fish-ponds.

In Europe macro-algae are grown in experimental fields, and natural basins. The capacity of macro-algae as bio-filters or nutrient uptake has been tested in the north-western Mediterranean Sea, along French coasts [7] using *Ulva lactuca* or *Enteromorpha intestinalis* that adapted to non-natural basins. Also in colder climate, macro-algae grow at a interesting rate. For example, in Denmark the Odjense Fiord produces ca. 10 kg per day of dry-weight-biomass, equal to a productivity of ca 10 t per year per hectare. Although macro-algae can grow in both hemispheres, the climatic factors may affect the productivity by reducing either the rate of growth or the growing-season. The Mediterranean area has ideal climatic conditions for a long growing season, with good solar irradiation intensity and year duration, and correct temperature. Moreover, along the coasts of several Countries (Italy, Spain, France, Greece) fishponds exist that may be the ideal localization of algae-ponds. Therefore, we have recently started a Project [8] aimed at assessing the potential of macro-algae as source of biofuel considering fishpond effluents as growing media.

Our objective is the use of recovered carbon dioxide from power plant flue gases or industrial plants as source of carbon.

A number of algae have been selected that, due to their adaptability to variable conditions and presence throughout the year, can be good candidate for cultivation in ponds. The selected algae have been investigated for the definition of the best conditions for their growth in a pond. The influence of temperature, irradiance, weight/volume ratio on the growth, and oxygen production has been followed during one year. Also, the production of oxygen by a freshly collected sample has been seasonally monitored as a function of the temperature. In this way, the best period for harvesting the algae can be defined and the wet collectible mass estimated.
Five algae have been treated so far, namely *C. linum, P. capillacea, U. rigida, C. vermilaria and G. bursa-pastoris.* Five different treatments can be used for the extraction of products. In this report we focus on the use of SC-CO_2 extraction, SC-CO_2 with methanol as co-solvent and the extraction with an organic solvent.

The equipment used for SC-CO_2 extraction was a SITEC apparatus, which temperature and pressure are fully computer controlled. The range of the working conditions is: temperature up to 500 K, pressure up to 33 MPa.
The organic solvent extraction was carried out with a Soxhlet apparatus using hexane as solvent. Because of the different permeability and resistance of the cell membrane of the tested algae, the use of either technique was not equally possible for all algae.

The cost of energy production from macro-algae depends on the biofuel content and the extraction technology. The estimate cost of feedstock may vary over a large interval, depending on the cultivation technique: typical values of 5 to 60 US$ per GJ of produced energy are usual. Such values are well over those of coal, oil, and LNG. Most recent revision of energy cost from macro-algae are as old as 1987 [9]. The productivity for macro-algae ranges from 150 to 600 t per hectare per year fresh weight, that is much higher than the typical value for sugarcane that ranges from 70 to 170 t_{fw} ha^{-1} y^{-1}. This means that under the best operative conditions macro-algae would be a better energy source than terrestrial biomass.
The minimum target value for a seaweed farm to be economically valuable is around 200 t per ha per year, that is higher than the productivity of micro-algae.
Interestingly, because of their edible use, several macro-algae have been fully characterized for their lipid content and nutritional properties. Consequently, a number of macro-algae are better characterized for their composition with respect to micro-algae. This also has contributed to gather useful information from the perspective of the evaluation of the biofuel productions. Noteworthy, depending on the algae species, a different composition of the extract is observed, that gives a different heat content to the fuel. It must be emphasized that methyl esters of acids may be used as fuels without any major problem.
The energetic value of the algae depends on the amount of compounds extracted that may be used as fuels. The content of fuels is very variable with the species considered, as it is the lipid content. A content of 10-20 % dw is quite usual, with a peak value up to 40%. Another key parameter to be evaluated for the assessment of the economic value of the macro-algae as source of biofuel is the energy that can be obtained from the extracted fuel. Such value allows to calculate the net energy (NE) obtainable from the algae, once it is known the energy needed for their growth (Eg), harvesting (Eh) and processing (Ep), Eq. 1.

$$\text{Net Energy} = \Delta H - (Eg + Eh + Ep) \qquad 1$$

We have also developed a tool for the evaluation of the approximate value of the heat content of the extracted material from algae and for evaluating the energetic yield of algae, not considering the dry residual material. Is worth to recall that, the residual algal mass after SC-CO_2 extraction is practically water free, and can, thus, find a use as fuel.

Taking into consideration the composition as acids and hydrocarbons, the average heat content of the algae used in this work was calculated to range around 11 500-13 500 kJ mol^{-1}, that corresponds to 24 000-30 000 kJ m^{-2} of sea surface.

Conclusions

Macro-algae are a promising source of renewable energy. In order to grow algae with an economic convenience for fuel extraction, R&D is necessary that will allow to establish the optimal growing condition, optimizing yield and minimizing costs. At least a fivefold reduction is necessary with respect to the actual cost for algae could be seriously considered as energy feedstock. Large ponds (10-20 hectare per pond, 1000 hectare surface) may produce a scale economy that will make convenient algae cultivation for energy extraction. The most convenient extraction technology must be selected for minimizing costs and for a better use of the entire algae mass.

Acknowledgement. The financial support by CNR-Rome Project CNRC008EBF is gratefully acknowledged.

References

(1) Kadam, K. L. *Energy Convers. Mgmt*., 1997, ***38***, PS 505-510.
(2) Wilde, E. W., Benemann, J. R.*Biotechnology Advances*, 1993, ***11***, 781-81.
(3) Gao, K., McKinley, K. R.,*J. Appl. Phycol*., 1994, ***6***, 45-60.
(4) Aresta, M., Dibenedetto, A., Tommasi, I., Cecere, E., Narracci, M., Petrocelli, A., Perrone, C., Elsevier 2002, Special Issue Dedicated to GHGT-6, Kyoto, October 2002.
(5) Cohen, I., Neori, A. *Bot. Mar.,* 1991, ***34***, 977-984.
(6) Hirata, H., Xu, B. SUISANZOSHOKU, 1990, ***38***, 177-182.
(7) Sauze, F. in "*Energy from Biomass*", Stub, A., Chartier, A., Schleser, P., Schleser, G. Eds, Elsevier Applied Science, London, 1983, p. 324-328.
(8) CNR-Rome, Agenzia 2000, Project CNRC008EBF
(9) Bird, K.T. in "*Seaweed Cultivation for Renewable Resources*", Bird, K. T. , Benson, P.H. Eds., Elsevier, Amsterdam, 1987, p. 327-350.

GENERATION OF NANOPOROUS THIN POLYMER FILMS VIA FOAMING WITH CARBON DIOXIDE

S. Siripurapu,[a] J.M. DeSimone,[a,b] R.J. Spontak[a] and S.A. Khan[a]

[a] Dept. of Chemical Eng., North Carolina State University, Raleigh, U.S.A.
[b] Dept. of Chemistry, University of North Carolina, Chapel Hill, U.S.A.

Abstract

We report the use of geometrical confinements to generate novel nanoporous thin polymer films with supercritical carbon dioxide ($scCO_2$). Poly(methyl methacrylate) films measuring on the order of 75-100 μm in thickness, when constrained between impenetrable plates in the foaming process yield a variety of diffusion-controlled foamed micro/nanostructures. Results obtained here demonstrate that the foamed cell size can be systematically reduced in such systems by applying high CO_2 saturation pressure and low temperature (near the T_g of the $scCO_2$-plasticized polymer). Cell sizes can also be lowered, and cell densities increased at lower CO_2 pressures, through the addition of a nanoscale filler or a tailored surfactant. Addition of such fillers enhances foaming through concurrent heterogeneous nucleation and/or decreasing the polymer- CO_2 interfacial tension, revealing that nanoporous polymers can be controllably generated through the synergistic use of diffusion control and filler/surfactant addition.

Introduction

The microcellular foaming process has been developed in the past to manufacture foamed products aimed at replacing their unfoamed analogs without compromising desired application-specific properties. In a typical microcellular foaming procedure [1], a polymer sample is saturated with an inert gas such as supercritical carbon dioxide $scCO_2$ at high pressures and desired foaming temperature. On reaching equilibrium of the gas uptake into the polymer, the gas is released in a controlled fashion near isothermal conditions to yield separation of the gas phase via nucleation and growth of gas bubbles to foam a stable foam structure. Microcellular foams of different thermoplastic materials have been generated in the past with $scCO_2$ in batch [1,2] and continuous [3,4] processes. Most studies in the past have concentrated on understanding the effects of foaming variables such as CO_2 saturation pressure, saturation time and foaming temperature on final foam cell sizes and nucleation densities [1]. Synthesis of nanoporous thin polymer films has become of significant interest recently due to potential novel applications such as low-*k* dielectrics, membranes and drug delivery vehicles [5]. Different synthesis approaches are being pursued utilizing block copolymers, nanotemplating and dentritic macromolecules [6]. The thin film geometry presents a challenge in achieving uniform nanoporous morphology in a foaming process due to depletion of the available CO_2 for nucleation through surface diffusion to the external environment. The main purpose of this work is (i) to investigate the use of simple geometrical constrains to incorporate uniform porosity in thin polymer films using a $scCO_2$-based foaming process and (ii) to study the effect of nanoscale fillers and tailored surfactants to achieve higher nucleation rates at lower CO_2 saturation pressures.

Experimental

Materials. The PMMA (Plexiglas VM-100) employed in this study was provided by Elf Atochem N.A. (King of Prussia, PA, U.S.A.) in pellet form and was purified before use in experimentation. Specific material properties are listed in Table 1. Carbon dioxide (>99.8% pure) was obtained from National Specialty Gases (Durham, NC, U.S.A.). Colloidal silica (particle diameter = 10-12 nm) dispersed as 30 wt% solution in methyl ethyl ketone was purchased from Nissan Chemicals Ltd. (Houston, Texas, U.S.A.). The non-ionic surfactants used in this study were synthesized using different techniques that will be described elsewhere. Table 2 gives specific details of the surfactant architectures.

Table 1: Polymer Characteristics

Polymer	M_n (kg/mol)	M_w (kg/mol)	M_w/M_n	Density (g/cm^3)	T_g (°C)
PMMA	70,000	107,000	1.53	1.18	101

Table 2: Surfactant Characteristics

Surfactant	M_n (kg/mol)	M_w/M_n
PMMA-*g*-PDMS (GCP)	40,000	1.46
PMMA-*b*-PFOMA (BCP1)	29k-b-3.5k	1.14
PMMA-*b*-PFOMA (BCP2)	110k-b-50k	1.2

Sample Preparation. Solutions of PMMA with/without the surfactants were prepared by dissolving 30 wt% polymer in toluene. Samples that included the nanoscale filler (colloidal silica) were prepared in methyl ethyl ketone. Thin films measuring 75-100 μm thick were formed by solution casting on a glass plate and drying under vacuum. The polymer films are separated from the glass plate under water and subsequently vacuum dried for an additional 12 h.

Foaming Experiments. The polymer films were cut into 1.3 cm x 2.5 cm samples for foaming experiments. A schematic of the foaming setup is shown in Figure 1. A sample film is sandwiched in the foaming die or placed alone in the foaming vessel. Once the vessel is heated to a desired foaming temperature in an oven, the sample is then saturated with CO_2 from an ISCO pump for a desired amount of time (6 h) at an elevated pressure (1000-5000 psi). The foaming vessel is finally depressurized rapidly to yield the final product.

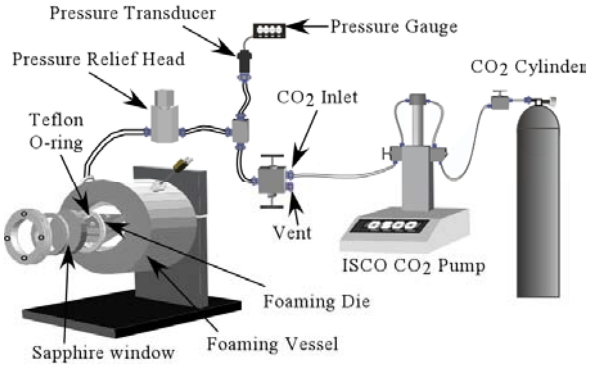

Figure 1. Schematic of the foaming setup

Foam Characterization. Foamed samples were dried under vacuum for 24 h at 50°C, fractured in liquid nitrogen and examined by scanning electron microscopy (SEM) with a Hitachi S3200N variable-pressure microscope. Backscattered electron images of uncoated foams were acquired at an accelerating voltage of 21 kV and a chamber pressure of 60 Pa. The images were subsequently analyzed for cell diameters, cell densities and the thickness of the unfoamed outer skin. While the cell diameter was taken as the

average of two dimensions in the cell, the cell density was determined using the method described elsewhere [2].

Results and Discussion

As a natural extension of the microcellular foaming process of bulk polymers, similar experiments have been attempted using thin polymer films. Figure 2 (a) shows a micrograph of a PMMA film foamed at 5000 psi and 40˚C. The foamed film is characterized by three regions, (i) a microcellular core, (ii) a transition region between the core and unfoamed skin and (iii) relatively thick unfoamed skins accounting for almost 70% of the film thickness. The microcellular core has a mean cell diameter of 1 μm and a cell density of *ca*. 10^{11} cells/cm^3 of material. Figure 2 (b) is an enlargement of the same sample showing the transition region and the unfoamed skin morphology. Attempts to optimize the process by varying process parameters such as foaming temperature and saturation pressure do not yield a substantial improvement in the ultimate foam morphology.

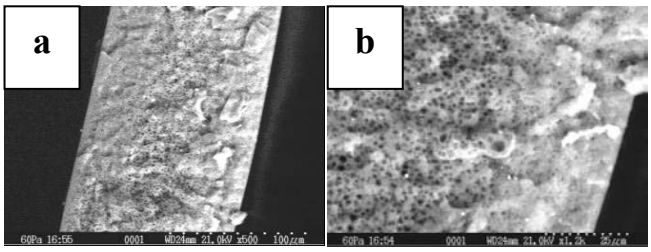

Figure 2. PMMA film foamed at 5000 psi and 40˚ C

Foaming with Diffusion Control. The fundamental difference between foaming bulk polymers and thin polymer films lies in the kinetics of the foaming process. Depressurization of the foaming cell results in nucleation of billions of microvoids in the polymer matrix. As a subsequent step, cell growth occurs wherein remaining gas in the polymer migrates to nuclei, thereby leading to the final microcellular structure upon retrograde vitrification of the polymer. In the case of thin films, there is competing gas diffusion occurring on the order of the same time scale as cell growth from the film surfaces. Such diffusion depletes available gas for cell growth. These two opposing transport mechanisms account for a high degree of heterogeneity in material properties such as viscosity, T_g, gas concentration and diffusion coefficients along the film thickness. This heterogeneity in combination with varying processing conditions, such as differences in foaming temperature, yield highly non-uniform foamed structures. Restricting surface CO_2 diffusion is anticipated to allow for greater gas availability for cell growth and higher uniformity of cell distribution.

To test the above hypothesis, a foaming die has been designed and machined with smooth surfaces that, when sandwiching the polymer film, serves as a physical constraint to CO_2 diffusion from the film surfaces. Figure 3(a) shows a micrograph of a PMMA film foamed under the same conditions as the sample in Figure 2, but in the presence of a diffusion barrier. The foamed film is characterized by extreme uniformity in cell size distribution and a ultrathin layer (corresponding to a single layer of cells) of unfoamed skin with a smooth integral surface, as seen in Figure 4(b). Confinement of the film in the foaming die eliminates property gradients across the film and promotes uniform cell growth, yielding a nanoporous foamed film with ultrathin unfoamed skin.

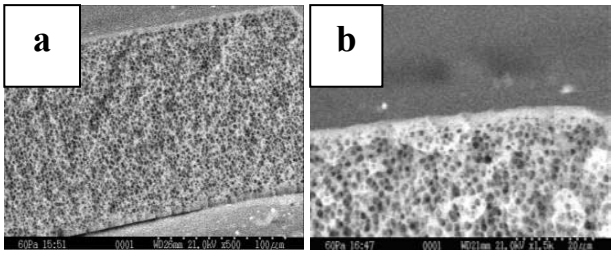

Figure 3. PMMA film foamed at 5000 psi and 40˚ C with diffusion control

Addition of nanoscale fillers and tailored surfactants. Nucleating agents such as talc are normally used in the foaming industry to achieve higher nucleation rates. We have attempted a synergistic combination of external confinement in the foaming die and nanoscale internal confinements via addition of colloidal silica (particle diameter = 10-12 nm) and the above-mentioned surfactants to enhance gas nucleation under various foaming process conditions. The rationale behind using the above surfactants is to have a block that is miscible in the polymer and a second block that has a strong CO_2-philicity (PDMS or PFOMA). We find the highest improvement in cell nucleation densities and uniform cell growth with the addition of the lower molecular surfactant (BCP1), even with liquid CO_2. Results from these studies will be discussed and guidelines for ideal surfactant architectures for different foamed morphologies will be given.

Conclusions

We have developed a new processing strategy to produce nanoporous thin polymer films using a gas foaming process with CO_2. The strategy involves physical restriction of gas diffusion from the film surfaces, allowing for higher gas availability for growth of stable nuclei. The resultant foams not only exhibit remarkably uniform pore morphologies at different length scales depending on the processing conditions, but also possess amazingly thin unfoamed skins. This process methodology has been improved to promote higher nucleation rates at lower CO_2 pressures via addition of a nanoscale filler or a tailored non-ionic surfactant that can influence the polymer- CO_2 interface.

Acknowledgement. This study was supported by the Kenan Center for the Utilization of Carbon Dioxide in Manufacturing and the STC Program of the National Science Foundation under Agreement No. CHE-9876674.

References

(1) Goel S.K. and Beckman E.J. *Polym. Eng. Sci.* **1993**, *34*, 271.
(2) Kumar V. and Weller J. E. *Polymeric Foams: Science and Technology* **1997**, American Chemical Society, Washington DC.
(3) Behravesh A.H., Park C. B. and Venter R. D. *Proc. ANTEC '98* **1998**, 1958.
(4) Siripurapu S., Gay Y. J., Royer J. R., DeSimone J. M., Spontak R. J. and Khan S. A. *Polymer* **2002**, *43*, 5511.
(5) Krause B., Mettinkhof R., van der Vegt N. F. A and Wessling M. *Macromolecules* **2001**, *34*, 874.
(6) Hawker C.J., Hedrick J.L., Miller R.D. and Volksen W. *MRS Bulletin 2000*, *25*, 54.

SELECTIVE CONVERSION OF CO_2 TO ETHYLENE BY THE ELECTROLYSIS AT A THREE-PHASE(GAS/LIQUID/SOLID) INTERFACE IN AN ACIDIC SOLUTION CONTAINING CUPRIC IONS

Kotaro Ogura, Hiroshi Yano, and Fukutaro Shirai

Department of Applied Chemistry, Yamaguchi University,
Tokiwadai Ube 755-8611, Japan

Introduction

We have previously reported that the electrochemical reduction of CO_2 at the three-phase (gas/liquid/solid) interface on a Cu-mesh electrode leads to the formation of major products such as CO, C_2H_4 and CH_4 with high current efficiencies and the deposition of poisoning species is extremely suppressed during the reduction.[1] These beneficial results are caused by the maintenance of high concentration of CO_2 at the three-phase interface in acidic solution. Hitherto, the electrochemical reduction of CO_2 has been performed mainly at the two-phase (liquid/solid) interface with an electrode wholly immersed into electrolyte in which CO_2 is supplied to the electrode through solution. Although a copper electrode shows a high catalytic activity toward the conversion of CO_2 to hydrocarbons with such an electrode in a neutral buffer solution,[2,3] the faradaic efficiencies are known to rapidly decrease after the start of electrolysis and the catalytic activity to disappear almost completely at longer times. This is caused by the deposition of poisoning species.[4,5] In general, neutral buffer solution has been used in such an electrolysis at the two-phase interface, because the hydrogen evolution is predominant in acidic solution and the reduction of CO_2 is difficult due to the insufficient concentration of protons in alkaline solution. As previously pointed out, however, the poisoning process including the deposition of graphitic carbon is expedient in a neutral solution.

In the present study, the electrolysis of CO_2 at the three-phase interface on a copper-mesh electrode was carried out in acidic halide solutions containing cupric ions, and the selective formation of ethylene was observed with a maximum Faradaic efficiency of 73.5% at –2.4V vs Ag/AgCl in a KBr solution of pH 3.

Experimental

The electrolysis cell used was schematically shown in **Figure 1**. The three-phase interface was constructed on a pure copper-mesh (purity 99.99%, 50 mesh, Nilaco Co.). The copper mesh put on a glass filter (average pore size, 20μm) was bound to a Teflon cylinder tightened with a Teflon cap. The cylinder with the copper-mesh was attached to a cathode compartment via an O-ring, which was separated from an anode compartment by a cation-exchange membrane (Selemion CMV 10, Asahi Glass Co.). The bottom of the Teflon cap was fixed to a reservoir containing the same solution as that used in the cathode compartment via an O-ring. The purified CO_2 gas was blown up onto the Cu-mesh through the glass filter from the bottom of the cell, and the reaction gas was circulated via the cathode compartment with a circulating pump. The gas/liquid/solid phase provided on the Cu-mesh electrode was sustained during the electrolysis by adjusting the rate of CO_2 flow, and the net surface area was 10.2cm^2. Before each experiment, the Cu-mesh electrode was immersed to remove Cu oxide in concentrated HCl, and washed with doubly distilled water and then with electrolytic solution in an ultrasonic bath. A platinum plate and an Ag/AgCl/saturated KCl electrode were used as the counter and reference electrodes, respectively. The electrolytes used were 3M KCl or KBr solutions

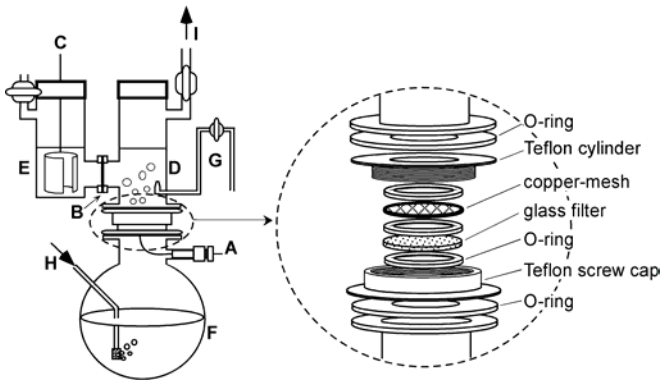

Figure 1 Schematic diagram of an electrolysis cell. A, working electrode (copper-mesh); B, cation-exchange membrane; C, counter electrode; D, cathode compartment; E, anode compartment; F, reservoir; G, Luggin capillary; H, gas inlet; I, gas outlet.

containing various concentrations of $CuSO_4$. The anolyte was always a 0.5M $KHSO_4$ solution of pH 0.

Gaseous products were analyzed with a Shimazu GC-8AIT and a GC-8AIF gas chromatograph. A Shimazu GC-MS spectrometer and an organic acid analyzer were used to analyze aqueous products. The electrode surface after the electrolysis was observed by FE-SEM and EPMA techniques.

Results and Discussion

The electrolysis of CO_2 was performed at the three-phase interface on a Cu-mesh electrode in a KCl solution of pH 3.0, and the Faradaic efficiency for each product is shown in **Figure 2** where the current density observed was : e. g., at –1.8V, 9.1~9.4mA/cm^2. The onset potential for the reduction of CO_2 was –1.4V, and the major products were C_2H_4, CH_4 and CO. Maximum Faradaic efficiencies for C_2H_4, CH_4 and CO were obtained at –1.8V: 46.3% (C_2H_4); 19.9% (CH_4); 18.0% (CO). The Faradaic efficiency for H_2 decreased with

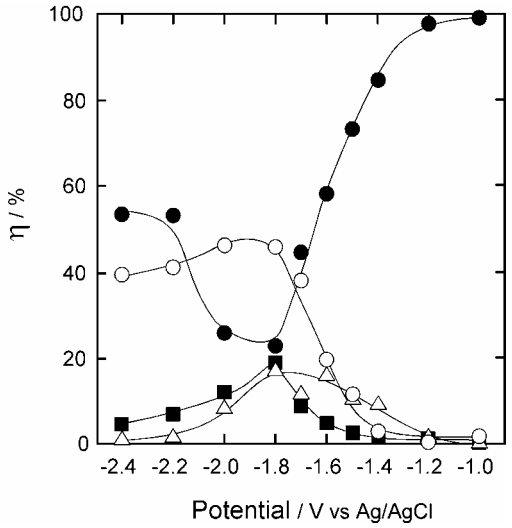

Figure 2 Plot of the Faradaic efficiencies for C_2H_4 (○), CO (△), CH_4 (■) and H_2 (●) versus the electrode potential in a 3M KCl solution of pH 3. Electrolysis time at each potential, 30 min.

Table 1 Faradaic efficiencies for the products obtained in the electrochemical reduction of CO_2 in a 3M KCl solution of pH 3 containing various concentrations of $CuSO_4$ on a Cu-mesh electrode[a)]

$CuSO_4$	Faradaic efficiency / %									Conversion[b)]	Selectivity[c)]	Q[d)]	η[e)]
mmol dm^{-3}	Ethylene	Methane	CO	Ethane	EtOH	Formic	Acetic	Lactic	H_2	%	%	C	%
0	46.3	19.9	18.0	1.1	0.0	2.5	0.4	0.0	23.1	4.5	37.3	177	111
0.01	49.9	20.2	11.3	0.6	0.0	2.6	0.6	0.8	24.3	6.9	45.6	205	110
0.05	52.4	6.1	9.5	1.2	0.2	3.2	0.3	0.2	26.9	7.1	54.0	242	100
0.3	56.5	4.8	5.5	1.0	0.0	3.0	0.2	0.1	33.1	7.0	64.8	267	104
0.5	58.1	4.0	4.6	1.3	0.3	3.7	0.6	0.0	35.5	7.2	65.8	274	108
1.0	61.0	5.5	4.6	1.0	3.5	3.4	0.7	0.6	37.9	7.2	64.0	262	118
1.5	50.5	0.9	4.9	2.6	1.2	2.7	0.4	0.3	41.5	7.5	64.5	358	105

a) Electrolyte,3M KCl containing $CuSO_4$, initial pH, 3.0; the area of a copper-mesh substrate, 10.2 cm^2; electrolysis potential, -1.8V vs Ag/AgCl; electrolysis time, 30 min; initial volume of CO_2, 480 cm^3; catholyte, 205 cm^3.
b) Conversion percentage in the electrolysis at 30 min.
c) Selectivity for the formation of ethylene on the basis of C content.
d) Amount of the electric charge passed in the electrolysis.
e) Total current efficiency in the reduction.

decreasing the potential and showed a minimum value of 20% at –1.8V. Beyond this potential, however, the formation of H_2 was again enhanced, and η reached 52.1% at –2.4V. The total Faradaic efficiency including that for hydrogen evolution was about 100% at each potential. Hence, it is indicated that there was neither unknown product nor poisoning species except for the compounds measured here.

As shown in **Table 1**, the product distribution is considerably affected by the addition of cupric ions to the electrolyte. The Faradaic efficiency for C_2H_4 increased with an increase in concentration of Cu^{2+} until 1mM, and the maximum value of η was 61.0%. Conversely, η for CH_4 and CO were about one fourth as large as those in the absence of Cu^{2+}. On the other hand, the Faradaic efficiency for C_2H_4 was always larger than that for H_2, although the hydrogen evolution was also enhanced by the addition of Cu^{2+}. The results also indicate that the addition of cupric ions was not accompanied by any poisoning reaction. This was supported from the EPMA data in which no any element except copper atom was detected on the electrode after the electrolysis.

In **Figure 3**, the conversion percentage of CO_2 and the Faradaic efficiency of each product are shown versus the electrode potential in a 3M KCl solution containing 1mM $CuSO_4$. The onset potential for the reduction of CO_2 was found to be –1.4V, and the conversion percentage increased linearly as the potential was shifted to the negative side. The current efficiency for ethylene reached a constant value of 65% at about –1.8V, but that for the hydrogen evolution dropped below 20% at –2.4V. Similar result was obtained for the electrochemical reduction of CO_2 in a 3M KBr solution with cupric ion. In a KI solution, however, the conversion percentage of CO_2 and the faradaic efficiency for C_2H_4 both were rather higher than those obtained in KCl solution (**Figure 3**); e. g., conversion percentage: 23.8% (KI), 20.5% (KCl) at –2.4V; faradaic efficiency for C_2H_4: 72.6% (KI), 66.0% (KCl) at –2.4V. Electron probe microanalysis of the electrode which had been used for the electrolysis of CO_2 in halide solutions containing $CuSO_4$ proved that cuprous halides were deposited on the copper-mesh electrode during the electrolysis. Especially, the existence of CuI was extremely evident from a definite EPMA spectrum. Hence, it is suggested that a cuprous halide is deposited *in situ* during the cathodic reduction and this species is involved as a catalyst in the conversion of CO_2 to ethylene.

Thus, the electrochemical reduction of CO_2 at the three-phase

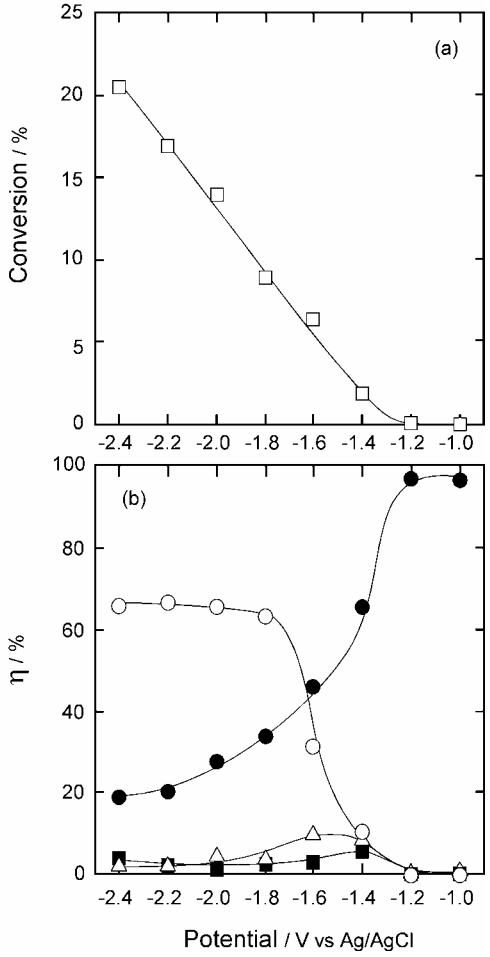

Figure 3 Plots of the conversion percentage of CO_2 (a) and the Faradaic efficiencies (b) for C_2H_4 (○), CO (△), CH_4 (■) and H_2 (●) versus the electrode potential in a 3M KCl solution of pH 3 containing 1mM $CuSO_4$. Electrolysis time at each potential, 30 min. Initial volume of CO_2, 480 cm^3.

interface led to the selective formation of C_2H_4 in a halide solution containing cupric ions. The probable reaction scheme is considered as: CO_2(g) is first reduced to CO(g) at the three-phase interface, CO adsorbs on a newly formed copper surface, and the electrochemical hydrogenation of CO to :CH_2 and the coupling of methylene radicals to C_2H_4 are followed. This would be brought about by the ability of copper halide which can combine reversibly with CO and C_2H_4 through their π bonds.[6]

References

1. H. Yano, F. Shirai, M. Nakayama, K. Ogura, *J. Electroanal. Chem.*, **2002**, 519, 93.
2. Y. Hori, K. Kikuchi, S. Suzuki, *Chem. Lett.*, **1985**, 1695.
3. J. J. Kim, D. P. Summers, K. W. Frese Jr., *J Electroanal. Chem.*, **1988**, 245, 223.
4. G. Kyriacou, A. Anagnostopoulos, *J. Electroanal. Chem.*, **1992**, 328, 233.
5. B. D. Smith, D. E. Irish, P. Kedzierzawski, J. Augustynski, *J. Electrochem. Soc.*, **1997**, 144, 4288.
6. H. Y. Huang, J. Padin, R. T. Yang, *Ind. Eng. Chem. Res.*, **1999**, 38, 2720.

Production of Synthesis Gas from H_2O and CO_2 with Nonthermal Plasma

Shigeru Futamura and Hajime Kabashima

National Institute of Advanced Industrial
Science and Technology
AIST Tsukuba West, 16-1 Onogawa, Tsukuba, Ibaraki,
305-8569 Japan

Introduction

The average global ground temperature has been increasing by 0.6±0.2˚C since 1861, and the contribution of CO_2 occupies ca 64 %.[1] Recognition of the CO_2 influence on the accelerated global warming[1] stimulated researches relevant to the development of technologies for the capture, sequestration,[2] and fixation of CO_2 along with those for energy conservation.

Many of CO_2 fixation technologies are still in the phase of fundamental research. Photochemical reduction of CO_2 to CO is achieved with some of rhenium complexes,[3] but UV light is necessary in the complicated processes of CO_2 reduction and the quantum yield is lower than unity. Direct methanol synthesis from CO_2 is possible with Cu/ZnO based catalysts at 200 ~ 300˚C.[4] However, this reaction is not cost-effective because a high pressure of H_2 [5.0 MPa of H_2/CO (3:1 v/v)] derived from electrolysis is assumed to be the H_2 source.

Recently, we have been applying nonthermal plasma to H_2 production from small molecules such as water,[5,6] methane,[6] and methanol,[6] and steam reforming of light paraffins such as methane, [7,8] ethane,[8] propane,[8] and 2,2-dimethylpropane.[8] In H_2 production, the substrate reactivity decreases in the order: methanol > methane > water. In the steam reforming of light paraffins, methane is the most desirable substrate because the highest H_2 yield is obtained with almost quantitative recovery of carbon atoms in the presence of sufficient water. The technical merits of nonthermal plasma consist in rapid start-up time and convenient operation at ambient temperature. It has been shown that the energy efficiency of the reactor is highly affected by the plasma-generating methods.[5-8]

These results urged us to explore the possibility of H_2O-CO_2 as an alternative substrate system to give synthesis gas in the reforming with nonthermal plasma. This paper will present the novel results on the reactor effect on the reaction behavior of H_2O-CO_2, product yields as functions of SED, water concentration dependence of product yields, $[H_2]/[CO]$, and carbon balance, and the successful results of a continuous operation.

Experimental

A ferroelectric packed-bed reactor (**FPR**) and a silent discharge reactor (**SDR**) used in this research were described in detail elsewhere.[9,10] Gas flow rate was set at 100 mL min^{-1} (residence time 44.5 s) and 50 mL min^{-1} (residence time 3 s) for **FPR** and **SDR**, respectively. The both reactors employed 50 Hz ac and high voltage up to 8 kV was applied to both of them. No breakdowns occurred during operations within their maximum voltages. CO_2 balanced with N_2 in a standard gas cylinder was introduced to the reactor through a Teflon tube by adjusting the CO_2 concentration and flow rate with sets of mass flow controllers after humidification in a water-bubbler in a thermostatic bath. Water concentrations were determined with a dew point hygrometer, and they were controlled within the range of 0.5 ~ 2.5 %. The gas streams passed through the entry tube (1/8 inch in diameter) and dispersed into the plasma zone as shown in Fig. 1. Reforming of H_2O and CO_2 was carried out at room temperature and an atmospheric pressure by using a conventional mass flow reaction system.

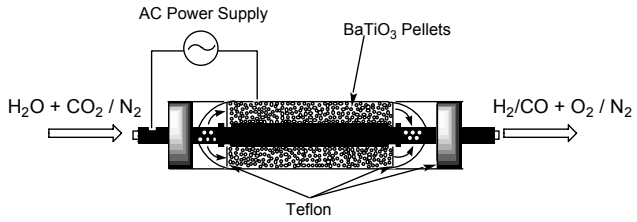

Figure 1. Schematic of ferroelectric pellets packed-bed reactor (**FPR**).

H_2 and methane were quantified by a TCD-GC with a packed column of Molecular Sieve 13X. CO, CO_2, ethane, ethylene, and acetylene were quantified by a GC equipped with a TCD and a FID with a packed column of Porapak Q+N and Molecular Sieve 13X.

Results and Discussion

Definitions of SED and the yields of H_2, CO, and O_2. As a measure of energy density for **FPR** and **SDR**, specific energy density (SED) will be used later (1), where Power denotes the plug-in power. The yields of H_2, CO, and O_2 are defined in (2), (3), and (4), respectively.

$$\text{SED (kJ L}^{-1}) = \text{Power (kW)} / [\text{Gas flow rate (L/min)} / 60] \quad (1)$$

$$H_2 \text{ yield (mol\%)} = 100 \text{ X } [H_2 \text{ concentration (ppm)} / \text{initial } H_2O \text{ concentration (ppm)}] \quad (2)$$

$$\text{CO yield (mol\%)} = 100 \text{ X } [\text{CO concentration (ppm)} / \text{initial } CO_2 \text{ concentration (ppm)}] \quad (3)$$

$$O_2 \text{ yield (mol\%)} = 200 \text{ X } [O_2 \text{ concentration (ppm)} / \{[H_2O]_{initial} + [CO]_{initial} \text{ (ppm)}\}] \quad (4)$$

Reactor Effect on the Reaction Behavior of H_2O-CO_2. Table 1 shows the reactor effect on the reaction behavior of H_2O - CO_2 in N_2 at 12 kJ L^{-1}. The gas flow rates for **FPR** and **SDR** were set at 100 mL min^{-1} and 50 mL min^{-1}, respectively.

Table 1. Reactor Effect on CO_2 Conversion and Product Distribution

Reactor	CO_2 Conv. (mol%)	Product yield (mol%)			$[H_2]/[CO]$
		H_2	CO	O_2	
FPR	12.3	12.4	11.8	2.8	2.1
SDR	0.5	0.7	>0.5	-	-

Initial concentrations of H_2O and CO_2 were 2.0 % and 1.0 %, respectively. Background gas N_2; SED 12.0 kJ L^{-1}.

A 24.6-fold higher CO_2 conversion was obtained with **FPR** than with **SDR**. Since the lifetime of the energetic electron is shorter than 100 ns, these data cannot be rationalized by the residence time difference between **FPR** and **SDR**. Similar types of barrier discharge plasmas are attained in both the reactors, but it is considered that electrons with higher energies are more highly populated in **FPR** than in **SDR**.[5-8] Based on these results, only **FPR** was used as a reactor in the subsequent reactions.

Irrespective of the reactor type, comparable yields were obtained for H_2 and CO. In the case of **FPR**, the O_2 yield was much lower than that of H_2. In the case of **SDR**, the O_2 amount was below the detection limit.

The yields of H_2, CO, and O_2 increased with SED. Irrespective of SED, almost the same yields were obtained for H_2 and CO. The O_2 yield was much lower than those of H_2 and CO.

H_2O Concentration Effect on the Product Distribution. Figure 2 shows the plot of CO yield vs. CO_2 conversion. The slope of the dotted line is unity, and the data points on this line show that the carbon atoms in the reacted CO_2 are quantitatively recovered as CO. In the absence of H_2O, CO yield saturates at 85 % with an increase in SED. Meanwhile, a good carbon recovery is obtained on addition of H_2O. The stoichiometry of the CO_2 deoxygenation process shows that a half amount of O_2 is produced compared to that of CO, but the data in Fig. 2 suggest the occurrence of the further deoxygenation of CO, resulting in lower carbon recovery. H_2O itself or its oxygen atoms may be involved in the oxidation of carbonaceous materials derived from CO_2.

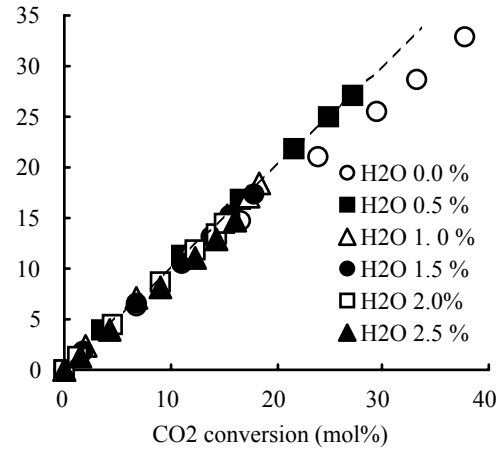

Figure 2. Carbon Balance in the Reaction of H_2O-CO_2 in N_2. Reactor **FPR**; CO_2 1.0 %; gas flow rate 100 mL min^{-1}.

Figure 3 shows the molar ratio of H_2 to CO as a function of SED. This ratio depends on the H_2O concentration, but almost the same ratios are obtained, irrespective of SED. These data suggest that compositions of synthesis gas from H_2O-CO_2 mixtures can be controlled by selecting pertinent ratios for initial concentrations of H_2O and CO_2. This trend sharply contrasts with those observed in the steam reforming of light paraffins.[5-8] In this reaction, deoxygenations of CO_2 and H_2O proceed independently from each other.

Continuous Production of H_2 and CO from H_2O-CO_2. Continuous operation of **FPR** in the reforming of H_2O-CO_2 in N_2 for 5 h (SED at 11.9 to 12.6 kJ L^{-1}) gave constant yields of H_2 and CO in about 12 % and 10 %, respectively, as observed in the steam reforming of methane.[5]

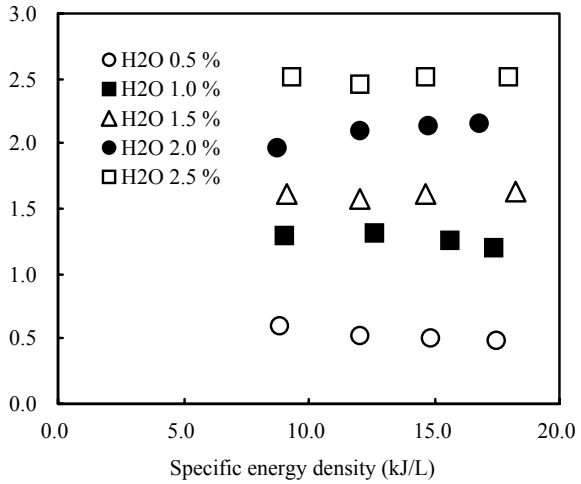

Figure 3. Effect of H_2O Concentration on the Molar Ratio of H_2 to CO in the Reaction of H_2O and CO_2.
Reactor **FPR**; CO_2 1.0 %; gas flow rate 100 mL min^{-1}.

In this process, target compositions of synthesis gases could be obtained by selecting pertinent ratios of H_2O and CO_2 depending on purposes such as H_2 utilization and preparation of a feedstock for methanol synthesis. At this moment, initial concentrations of H_2O and CO_2 cannot be increased due to the occurrence of the backward reaction of H_2 and O_2. Rapid separation of the products is mandatory to increase the potential of this method.

Conclusions

It has been shown that a versatile process of synthesis gas production from H_2O-CO_2 can be constructed with nonthermal plasma. Good carbon balances are obtained, and the molar ratio of H_2 to CO can be facilely controlled by changing the initial concentration ratios of H_2O and CO_2. Continuous operation of **FPR** for 5 h assured the constant yields of H_2 and CO.

Acknowledgment. This work was partly supported by the Grants-in-Aid from New Energy and Industrial Technology Development Organization of Japan (NEDO).

References

(1) 2nd Assessment Report of IPCC, 1997.
(2) Kajishima, T.; Saito, T.; Nagaosa, R.; Kosugi, S. *Energy*, 1997, **22**(2/3), 257.
(3) Hawecker, J.; Lehn, J.-M.; Ziessel, R. *Helv. Chim. Acta*, 1986, **69**, 1990.
(4) Saito, M.; Fujitani, T.; Takeuchi, M.; Watanabe, T. *Appl. Catal. A: General*, 1996, **138**, 311.
(5) Kabashima, H.; Einaga, H.; Futamura, S. *Chem. Lett*., 2001, 1314.
(6) Kabashima, H.; Einaga, H.; Futamura, S. *IEEE Trans. Ind. Applicat*., in press.
(7) Kabashima, H.; Futamura, S. *Chem. Lett*., 2002, in press.
(8) Futamura, S.; Kabashima, H.; Einaga, H. *IEEE Trans. Ind. Applicat*., submitted for publication.
(9) Futamura, S.; Zhang, A.; Yamamoto, T. *IEEE Trans. Ind. Applicat*., 2000, **36**(6), 1507.
(10) Einaga, E.; Ibusuki, T.; Futamura, S. *IEEE Trans. Ind. Applicat*., 2001, **37**(5), 1476.

On the mechanism of synthesis of acetic acid directly from CH_4 and CO_2 Using Dielectric-barrier Discharges

Chang-jun Liu[1], Jian-guo Wang[1], Yu Wang[1] and Baldur Eliasson[2]

[1]ABB Plasma Greenhouse Gas Chemistry Laboratory, State Key Laboratory of C1 Chemistry and Technology, Tianjin University, Tianjin 300072, China
[2]ABB Switzerland Ltd., CH5405, Baden, Switzerland

Introduction

The synthesis of acetic acid directly from methane and carbon dioxide is a 100% atomic economic reaction:

$$CH_4+CO_2 \rightarrow CH_3COOH, \quad \Delta G°_{400\ K} = 19.2\ kcal/mol \qquad (1)$$

The reaction is not favored thermodynamically. Huang et al. proposed a two-step conversion of methane into acetic acid [1]. With the first step, methane is adsorbed in the catalyst. Then, in the second step, the adsorbed methane species react with carbon dioxide to make acetic acid. The main obstacle is presented by thermodynamics rather than kinetics. A periodic operation has been proposed to break the thermodynamic limitations [1]. Regarding this thermodynamic limitation, the gas discharge plasma can be applied for thermodynamically un-favored reactions. We previously reported a direct synthesis of acetic acid from methane and carbon dioxide using dielectric-barrier discharges (DBDs) [2,3]. A yield of up to 2.7% of acetic acid has been achieved. The discharge plasma has been confirmed to be an effective way to make the reaction (1) become true even at ambient conditions. However, the reaction mechanism for such acetic acid synthesis remains unclear. To improve the synthesis, it is very necessary to investigate the reaction mechanism theoretically. In this work, we use the three hybrid DFT methods to study the reaction mechanism of the formation of acetic acid. Several routes of dissociation of CO_2 have been discussed. The main reaction pathways for acetic acid synthesis have been analyzed by using the three hybrid DFT methods. To confirm the mechanism, an experimental investigation has been conducted.

Computations

All the calculations have been performed with the Gaussian98 package [4]. The Becke's three parameters exchange functional [5] were used to combine with three different correlation functions: LYP [6,7], Perdew 86[8] and Perdew and Wang's 1991 gradient-corrected correlation functional[9,10]. The structures of all kinds of molecules and radical were optimized at the B3LYP, B3P86 and B3PW91 level with 6-311G(d, p) basis set. Vibrational frequency calculations were performed for each structure at the same level used for the geometrcal optimization. The potential energy surface was obtained by the Scan calculation.

Results and discussion

The simulation results show that there are two pathways for the synthesis of acetic acid directly from methane and carbon dioxide using dielectric-barrier discharges. One pathway is via CO_2^-, and the other is via the formation of CO. The first pathway requires less energy. Therefore the mechanism can be described as following.

When the reactants are fed into the discharge region, they can be dissociated due to the existence of electrons with energies ranged from 1 to10 eV [11,12]. The reaction is thereby initiated from the dissociation reactions of CH_4 and CO_2:

$$CH_4 \rightarrow CH_3+H \qquad (2)$$
$$e^-+CO_2 \rightarrow CO_2^- \qquad (3)$$
$$e^-+CO_2 \rightarrow O^-+CO \qquad (4)$$
$$e^-+CO_2 \rightarrow O+CO+e^- \qquad (5)$$

The reactions to produce acetic acid via the CO_2^- include:

$$CO_2^-+H \rightarrow COOH^- \qquad (6)$$
$$CH_3+COOH^- \rightarrow CH_3COOH+e^- \qquad (7)$$

Acetic acid can also be synthesized via CO:

$$CH_3+CO \rightarrow CH_3CO \qquad (8)$$
$$CH_3CO+O \rightarrow CH_3COO \qquad (9)$$
$$CH_3CO+O^- \rightarrow CH_3COO^- \qquad (10)$$
$$CH_3COO+H \rightarrow CH_3COOH \qquad (11)$$
$$CH_3COO^-+H \rightarrow CH_3COOH+e^- \qquad (12)$$

or

$$O+H \rightarrow OH \qquad (13)$$
$$O^-+H \rightarrow OH^- \qquad (14)$$
$$CH_3CO+OH \rightarrow CH_3COOH \qquad (15)$$
$$CH_3CO+OH^- \rightarrow CH_3COOH+e^- \qquad (16)$$

The detailed energy parameters calculated will be presented in the future publications.

We have previously reported the direct synthesis of acetic acid from methane and carbon dioxide using dielectric-barrier discharges [2,3]. The experiment has confirmed indirectly the first reaction pathway. To confirm the second reaction pathway, we conducted an experimental investigation using methane and carbon monoxide as the co-feed gases using the same reactor system as reported previously [2,3]. Table 1 presents the conversion of methane and carbon monoxide. It can be seen that the conversion is very high. Table 2 shows the composition of liquid product. Obviously, acetic acid can be produced this way. This confirms the second pathway experimentally.

Table 1. Conversions of methane and carbon monoxide

Ratio of CH_4/CO	2/1	2/1	1/1
Input power/W	50	100	100
Conversion of CH_4	43.74	62.45	72.92
Conversion of CO	14.70	20.02	18.51

Temperature of reaction: 338K; flow rate of feed: 40 ml/min

Table 2. Component of liquid products

Component	w%
Methanol	1.54
Ethanol	2.08
1-Propanol	2.51
2-Butanone	1.81
2-Butanol	3.07
Acetic acid	21.60
Propanoic acid	19.56
Butanoic acid	3.04
Pentanoic acid	1.22
Hydrocarbons	8.25

Temperature of reaction: 338K; flow rate of feed: 40 ml/min

Acknowledgments

The authors are grateful for supports from the Major Research Foundation of Ministry of Education of China (under the contract No. Major 0212) and ABB Corporate Research Ltd., Switzerland.

References

[1] W. Huang, K.-C. Xie, J.-P. Wang, Z.-H. Gao, L.-H. Yin and Q.-M. Zhu, J. Catal. **2001,** 201, 100.
[2] Y. Li, C.-J. Liu, B. Eliasson and Y. Wang, Energy Fuels **2002**, 16, 864.
[3] C.-J. Liu, Y. Li, Y.-P. Zhang, Y. Wang, J. Zou, B. Eliasson and B. Xue, Chem. Lett. **2001**, 1304.
[4] M. J. Frisch, G. W. Trucks, H. B. Schlegel, G. E. Scuseria, M. A. Robb, J. R. Cheeseman, V. G. Zakrzewski, J. A. Montgomery, Jr., R. E. Stratmann, J. C. Burant, S. Dapprich, J. M. Millam, A. D. Daniels, K. N. Kudin, M. C. Strain, O. Farkas, J. Tomasi, V. Barone, M. Cossi, R. Cammi, B. Mennucci, C. Pomelli, C. Adamo, S. Clifford, J. Ochterski, G. A. Petersson, P. Y. Ayala, Q. Cui, K. Morokuma, D. K. Malick, A. D. Rabuck, K. Raghavachari, J. B. Foresman, J. Cioslowski, J. V. Ortiz, A. G. Baboul, B. B. Stefanov, G. Liu, A. Liashenko, P. Piskorz, I. Komaromi, R. Gomperts, R. L. Martin, D. J. Fox, T. Keith, M. A. Al-Laham, C. Y. Peng, A. Nanayakkara, M. Challacombe, P. M. W. Gill, B. Johnson, W. Chen, M. W. Wong, J. L. Andres, C. Gonzalez, M. Head-Gordon, E. S. Replogle, and J. A. Pople, Gaussian 98, Revision A .9, Gaussian, Inc., Pittsburgh PA, 1998.
[5] A. D. Becke, J. Chem. Phys. **1993**, 98, 5648
[6] C. Lee, W. Yang and R. G. Parr, Physical Review B **1988**, 37, 785.
[7] B. Miehlich, A. Savin, H. Stoll and H. Preuss, Chem. Phys. Lett. **1989**, 157, 200.
[8] J.P.Perdew, Phys. Rev. B **1986**, 33, 8822.
[9] J. P. Perdew, in Electronic Structure of Solids '91, Ed. P. Ziesche and H. Eschrig (Akademie Verlag, Berlin, 1991) 11.
[10] J. P. Perdew, J. A. Chevary, S. H. Vosko, K. A. Jackson, M. R. Pederson, D. J. Singh and C. Fiolhais, Phys. Rev. B **1992**, 46.
[11] B. Eliasson, M. Hirth, U. Kogelschatz. J.Phys.D:Appl.Phys. **1987**, 20, 1421
[12] B. Eliasson, U. Kogelschatz. IEEE Trans.Plasma Sci. **1991**, 19, 309

STUDY OF CARBON FORMATION ON Ni-MgO CATALYST DURING REFORMING OF $^{13}CH_4$ WITH CO_2

Abolghasem Shamsi

U.S. Department of Energy
National Energy Technology Laboratory
P. O. Box 880
3610 Collins Ferry Road
Morgantown, WV 26507-0880

Introduction

Reforming is a critical technology that is necessary for generating cleaner fuels such as pure hydrogen and synthesis gas from coal, natural gas, and carbonaceous wastes. It is also compatible with the technologies used for capturing and sequestering CO_2. SynGas and hydrogen produced from fossil and renewable sources will play an important role in the 21st century, powering high-efficiency electricity generating systems, which are essential for reducing greenhouse gas emissions. SynGas could be converted to pure hydrogen (for fuel cells), low-sulfur liquid fuels, chemicals, and fuel additives. It has been reported that syngas production routes are efficient, but still expensive and the major problem is avoiding carbon formation.[1] Carbon is the major cause of catalyst deactivation and since the rate of carbon formation is greater than the rate of carbon gasification, carbon accumulates in the catalyst bed, causing catalyst deactivation and plant shutdown. Industrially, this problem is solved by addition of excess steam or oxygen, which increases the cost of syngas production. The cost of syngas production in a system that converts natural gas to liquid fuels is more than 60-70% of the total cost.[2] And the higher cost is mainly due to addition of excess steam or oxygen to the process for preventing carbon formation. Therefore, the challenge is to expand our understanding of the reforming process and to develop technologies that produce cheaper and cleaner energy in an environmentally acceptable manner.

It has been reported that a cost-reduction of 25% in syngas production would allow the gas-to-liquids processes to become more competitive with oil refining.[3] Therefore, developing catalysts and processes that operate at low steam/carbon and/or oxygen/carbon ratios would have a significant impact on the cost of syngas production. Increasing the life and the efficiency of the catalyst can also lower the cost of syngas production. Therefore, studies attempting to explain catalyst deactivation by carbon formation have intensified in recent years.

Numerous research groups have focused their efforts on reducing carbon formation during reforming reactions and their efforts have been carried out mainly at atmospheric pressure. However, several groups studied carbon formation at higher pressures. For example, Tomishige et al. have studied the effect of pressure on the reaction of methane with CO_2 over a Ni0.03Mg0.97O solid solution which, under atmospheric pressure, is resistant to carbon formation.[4,5] Our earlier studies with Pt/ZrO_2, $Pt/Ce\text{-}ZrO_2$, and Rh/Al_2O_3 catalysts also showed similar results.[6] With increasing pressure, methane and CO_2 conversion rates decreased, H_2/CO ratio decreased, and the rate of carbon formation increased. Higher rates of carbon formation at high pressure leads naturally to the question of whether the source of carbon at elevated pressures is the same as at 1 atmosphere. It is well known that most of the carbon deposited on the catalyst during reforming of methane with CO_2 comes from CO disproportionation and methane decomposition. Understanding which of these carbon sources is the major contributor at high pressure is necessary information in developing processes that will prevent or reduce carbon formation under industrial reaction conditions. Therefore, we have undertaken a ^{13}C-labeling study, using $^{13}CH_4$, to compare the relative contributions of methane and CO_2 as the sources of carbon formation at low and high pressures.

Experimental

The Ni-MgO catalyst was prepared by dissolving $Mg(NO3)2.6H_2O$ and $Ni(NO3)2.6H_2O$ (Ni/Mg = 0.5) in de-ionized water and mixing the solution on a hotplate until the excess water was removed. The resulting powder was heated in air at 850°C for two hours to decompose nitrates into oxides of MgO, NiO, Mg0.4Ni0.6O, and $MgNiO_2$ as indicated by x-ray diffraction. Before reaction the samples were reduced for two hours at 600°C under flowing hydrogen (30 ml/min) and tested at 800°C in a fixed-bed reactor with $^{13}CH_4/CO_2 = 1{:}1$.

Temperature-programmed oxidation (TPO) of deposited carbon was performed after the reaction by heating the sample from 30 to 900°C at a rate of 20°C/min in flow of 2% oxygen in helium (40 ml/min). Pulse reactions were performed by injecting 22.31 μmoles of reactant into He carrier gas (40 ml/min) at 800°C and pressures of one and 10 bar. The reaction products were analyzed and quantified by a quadrupole mass spectrometer using internal and external standards.

Results and Discussion

Reaction of $^{13}CH_4$ with CO_2 over reduced Ni-MgO at steady state conditions

Ni-MgO catalyst has been extensively studied for reaction of methane with CO_2 and it appears to be more resistant to carbon formation than other Ni-based catalysts, specifically in solid solution form.[5] Although there are some studies conducted at higher pressure the majority of the results are obtained at atmospheric pressure. Most of the downstream processes using syngas or hydrogen require compressed gases. Therefore it is more economical to conduct reforming reactions at higher pressure, which causes a serious problem due to high amount of carbon deposition. The Ni-MgO catalyst was tested at 800°C and at pressures of one and 10 bar. The carbon formed on the catalyst was quantified by oxidation of carbon and measuring the amount of CO and CO_2 produced. The results of temperature-programmed oxidation of carbon to CO_2 are shown in Figure 1, indicating that a significant amount of oxygen consumed by the catalyst at about 380°C compared to that consumed by carbon. As the time on stream increased the amount of carbon also increased at a rate of 15.7 mg-C/g-cat.h. The catalyst was regenerated and tested six times without any significant loss of activity or selectivity. Methane and CO_2 conversions of 96 and 94% were obtained, respectively, with a H_2 /CO ratio of 0.76.

Pulse reaction of $^{13}CH_4$ with CO_2 over reduced and oxidized Ni-MgO catalyst at 10 bar

A gas mixture with $^{13}CH_4/CO_2 = 1{:}1$ was injected over reduced and oxidized Ni-MgO catalyst at 800 °C and 10 bar (He at 40 ml/min used as carrier gas). Figure 2 shows the product distribution for the first pulse over the reduced catalyst. The H_2 concentration over the reduced sample was about 44% compared to 8% for the oxidized sample. The CO concentration (47%) was also higher for the reduced sample compared to that of oxidized one (15%). The peak maxima for H_2 and CO were delayed about 23 seconds compared to that of CO_2. Similar results were obtained with the oxidized sample with a time delay of about 16 seconds. The ratios for $^{12}CO_2/^{13}CO_2$ and $^{12}CO/^{13}CO$ were about 0.95 for both the reduced and oxidized samples. On the first pulse about 95% of methane and 80% of CO_2

were converted over the reduced sample compared to 80% of methane and 19% of CO_2 over the oxidized sample as shown in Figure 3. Methane and CO_2 conversions and the concentrations of H_2 and CO were increased with the second and third pulse over the oxidized sample. As a higher amount of CO_2 converted the concentrations of $^{12}CO_2$ and $^{13}CO_2$ decreased with increasing number of pulses. The product distributions over reduced sample showed smaller changes with increasing number of pulses. Methane appears to react readily with the oxidized sample where as CO_2 requires reduced sites for reaction to occur. Equal amounts of $^{12}CO_2$ and $^{13}CO_2$ were detected over both the reduced and the oxidized samples and the concentration of $^{13}CO_2$ follows the same trend as $^{12}CO_2$, indicating that the oxygen exchange reaction is very fast as reported earlier.[8]

$$^{12}CO + {}^{13}CO_2 = {}^{13}CO + {}^{12}CO_2$$

Five pulses of oxygen (22.31 7moles each) were introduced after the reaction to oxidize the deposited carbon on the catalyst and about 688 7moles/g.cat. were consumed by the catalyst. The major products were H_2 and H_2O with no significant amounts of carbon oxides, indicating that carbon deposition in the presence of CO_2 at 800°C and 10 bar was insignificant. Similar results obtained for the oxidized sample except that the catalyst consumed less oxygen (491 7moles/g.cat) after 4 pulses of oxygen. It appears that methane reacts with surface oxygen, reducing NiO to metallic nickel, and forming adsorbed CH_x, H_2, and OH. However, CO_2 requires reduced sites in order to dissociate into adsorbed oxygen (Oad) and CO or the CO_2 reacts with adsorbed hydrogen via reverse water gas shift reaction forming H_2O and CO. Furthermore, CO could also form from interaction of adsorbed CH_x and OH.[9] The results indicated that carbon deposited on the catalyst formed from both methane and CO_2, possibly via disproportionation of CO which is produced from both $^{13}CH_4$ and $^{12}CO_2$. The time delay observed for H_2 and CO could result from strong adsorption of these species on the reduced nickel sites.

Conclusions

Catalytic reaction of $^{13}CH_4$ with CO_2 over reduced and oxidized Ni-MgO catalyst was studied to obtained mechanistic information at low and higher pressures. No significant amount of carbon was deposited with reaction time of less than 60 minutes. However, as the time increased the amount of carbon deposited on the catalyst increased. The carbon deposited on the catalyst during the first hour of reaction appears to be very active and was removed by reacting with 2vol% oxygen in He at temperature of about 660°C. The catalyst maintained its original reactivity and selectivity after removal of carbon.

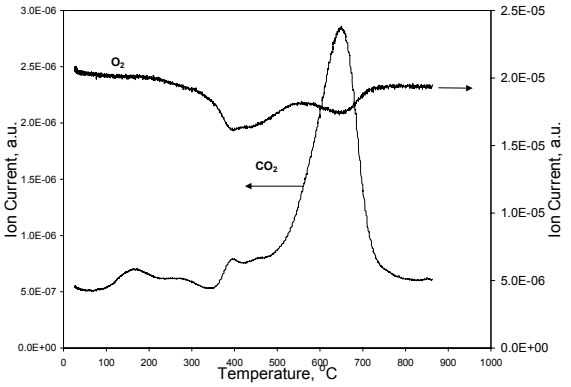

Figure 1. TPO of deposited carbon on Ni-MgO catalyst reacted at 800°C and 1 bar

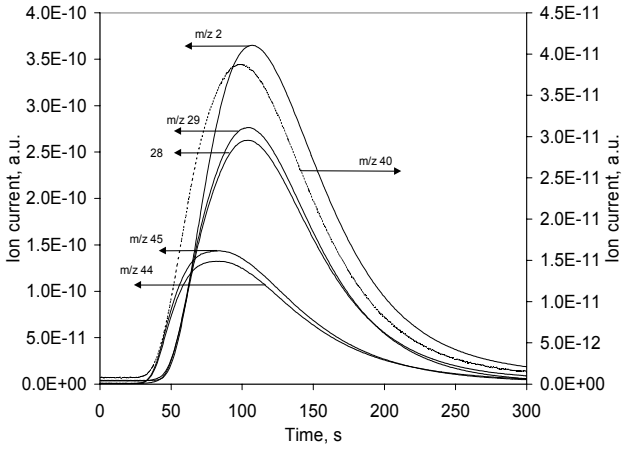

Figure 2. Pulse reaction of $^{13}CH_4/CO_2$ = 1:1 over reduced Ni-MgO catalyst at 800°C and 10 bar

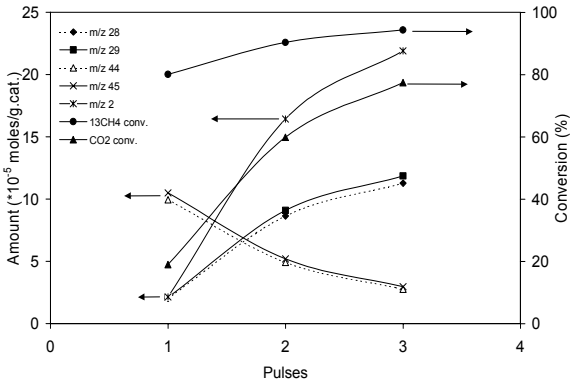

Figure 3. Pulse reaction of $^{13}CH_4/CO_2$ =1:1 over oxidized Ni-MgO catalyst 800°C and 10 bar

References

1. Jens R. Rostrup-Nelson, New aspect of syngas production and use, Catalysis Today 63 (2000) 159-164.
2. L. Basini and L. Piovesan, Ind. Eng. Chem. Res. 37 (1998) 258-266.
3. L. P. Lange and P.J.A. Tijm, Process for Converting Methane to Liquid Fuels: Economic Screening Through Energy Management, Chem. Eng. Sci. 51 (1996) 2379.
4. K. Tomishige, Y. Himeno, O. Yamazaki, Y Chen, T. Wakatsuki, K. Fujimoto, Kinetics and Catal. 40(3) (1999) 388-394.
5. K. Tomishige, Y. Himeno, Y. Matsuo, Y. Yoshinaga, K. Fujimoto, Ind. Eng. Chem. Res. 39 (2000) 1891-1897.
6. A. Shamsi, C.D. Johnson, Am. Chem. Soc., Div. Fuel Chem., Preprints, 46 (2001) 94-96.
7. D.Qin, J. Lapszewicz, Catalysis today 21 (1994) 551-560.
8. E. P. J. Mallens, J. H. B. J. Hoebink, and G. B. Marin, Journal of Catalysis 167 (1997) 43-56).
9. M.C.J. Bradford and M.A. Vannice, Applied Catalysis A: General 142 (1996) 97-122.

SYNTHESIS OF DIMETHYL CARBONATE AND PROPYLENE CARBONATE FROM UREA

Wang Mouhua, Zhao Ning, Yang Jinhai, Wei Wei, and Sun Yuhan

State Key Laboratory of Coal Conversion Institute of Coal Chemistry, Taiyuan 030001, China

Introduction:

Synthesis of urea was a traditional industrial process for CO_2 utilization. As a CO_2 carrier, urea was cheap and widely available, so it was thought to be a potential route for the synthesis of important organic compounds, such as dimethyl carbonate or propylene carbonate from urea.

Dimethyl carbonate(DMC) was environmentally benign in organic synthesis as intermediates substituting the poisonous phosgene and dimethyl sulfate. In addition, DMC could also be used as fuel additives to improve the combustion efficiency[1,2]. Propylene carbonate(PC) was important as an organic solvent, a processing agent for synthesis fibers, a raw material for a pharmaceutical composition or an intermediate for the synthesis of dimethyl carbonate[3]. At present, DMC was produced industrially by phosgene or by liquid-phase or gas-phase oxidative carbonylation of methanol; PC was produced by cycloaddition of CO_2 and propylene oxide. As a result, DMC and PC synthesis from urea has a lot of advantageous which was considered to be an alternative method such as cheap feedstock and low toxicity.

The known catalysts for the synthesis of DMC were organotin compound and alkali metal compounds. The known catalysts for the synthesis of PC were metal oxide. Cho reported the using of alkali metal compound or quaternary ammonium compound as catalyst, but the DMC yield was low[3]. The yield of DMC was 36.4% over LiH catalyst according to West[4]. Saleh obtained higher DMC yield and selectivity over dibutyl methoxy isocyanato tin catalyst[5]. High yield and selectivity of DMC was reached by using dibutyl dimethoxy tin and high boiling electron donor compound(triglyme) as cocatalyst[6]. However, the preparation of these catalysts was difficult and expensive. In addition, the separation of the products was also very complex. Thus, homogeneous catalysts should be disadvantageous to industrialization. The synthesis of propylene carbonate from urea and propylene glycol also had the same problems. The present paper investigated the performance of different metal oxide for the synthesis of dimethyl carbonate and propylene carbonate from urea.

Experimental:

A serious of metal oxides had been prepared and the catalytic activity for synthesis of DMC and PC were evaluated. The solid base MgO, ZnO, CaO were prepared by calcination of the corresponding hydroxide. The Bu_4Sn was used as commercial product prepared by Fluka. The synthesis of DMC was carried out in a novel reactor. In order to promote the selectivity and the yield of the products, the ammonia which was the by-product in the two reactions should be removed efficiently.

Results and discussion:

Figure 1 showed the effect of the catalyst on the yield of DMC from urea and methanol. It could be seen that the catalyst showed different performance on the synthesis of DMC from urea and methanol. When little catalyst was used, MgO showed the better results than ZnO. However, with the increasing of the catalyst weight, the DMC yield over ZnO increased dramatically which was higher than that of MgO and Bu_4Sn reported by Ryu. The different activity of these catalysts could be related to the base strength and base density of the catalysts.

Figure 2 illustrated the influence of the solid catalyst on the producing of PC from urea and propylene glycol. It was found that the metal oxide catalyst(MgO, ZnO) showed high yield to PC. Higher yield of PC over $Ca/K/SiO_2$ catalyst was also obtained while $Pb(Ac)_2$ and NaCl showed poor performance. It was obvious that the reaction results were also related to the basicity of the catalyst. How the basicity of the catalyst influence the reaction was under research

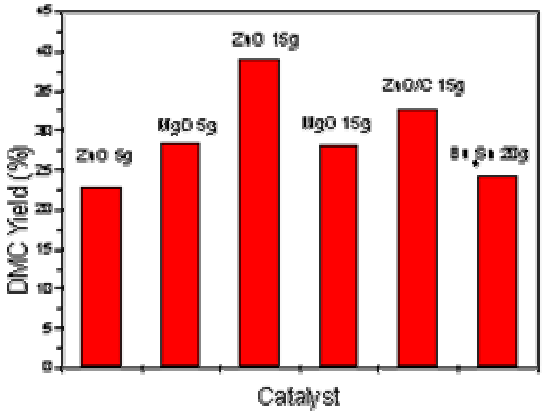

Fig.1 Effect of the catalyst on the DMC yield

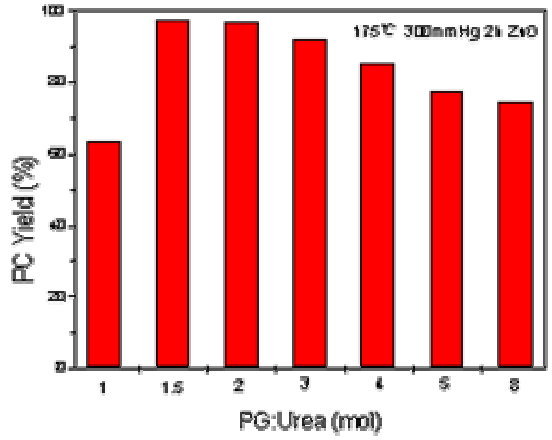

Fig.2 Effect of molar ratio of PG to urea on the reaction

It could be seen from the results that the solid base had the ability to promote the formation of PC and DMC from urea though the activity was different. The activation of the reactant might obey the same mechanism. The removal of the by-product ammonia was necessary to promote the selectivity and yield of the products. The novel reactor should be used. The synthesis of DMC and PC was thought to be a promising process for the utilization of CO_2.

References

(1) Ono.Y, *Applied Catalysis A*, **1997**, 155, 133.
(2) M,Ratzenhofer, *Angew.Chem. Int. Ed. Engl.,* **1980**, 19,317
(3) Cho, T. US 5534649 (**1994**)
(4) West. U. JP 10-109960 (**1998**)
(5) Saleh. R, WO 9517369 (**1995**)
(6) Ryu, J US 5902894(**1999**)